Front. Optoelectron. 2021, 14(2): 134–147
https://doi.org/10.1007/s12200-021-1220-6

REVIEW ARTICLE

Fundamentals and applications of spin-decoupled Pancharatnam–Berry metasurfaces

Yingcheng QIU[1], Shiwei TANG (✉)[1], Tong CAI[2], Hexiu XU[2], Fei DING (✉)[3]

1 School of Physical Science and Technology, Ningbo University, Ningbo 315211, China
2 Air and Missile Defense College, Air Force Engineering University, Xi'an 710051, China
3 Centre for Nano Optics, University of Southern Denmark, Campusvej 55, DK-5230 Odense M, Denmark

Abstract Manipulating circularly polarized (CP) electromagnetic (EM) waves at will is significantly important for a wide range of applications ranging from chiral-molecule manipulations to optical communication. However, conventional EM devices based on natural materials suffer from limited functionalities, bulky configurations, and low efficiencies. Recently, Pancharatnam–Berry (PB) phase metasurfaces have shown excellent capabilities in controlling CP waves in different frequency domains, thereby allowing for multi-functional PB meta-devices that integrate distinct functionalities into single and flat devices. Nevertheless, the PB phase has intrinsically opposite signs for two spins, resulting in locked and mirrored functionalities for right CP and left CP beams. Here we review the fundamentals and applications of spin-decoupled metasurfaces that release the spin-locked limitation of PB metasurfaces by combining the orientation-dependent PB phase and the dimension-dependent propagation phase. This provides a general and practical guideline toward realizing spin-decoupled functionalities with a single metasurface for orthogonal circular polarizations. Finally, we conclude this review with a short conclusion and personal outlook on the future directions of this rapidly growing research area, hoping to stimulate new research outputs that can be useful in future applications.

Keywords spin-decoupled, Pancharatnam–Berry (PB) metasurfaces

1 Introduction

Metasurfaces, the two-dimensional artificial interface composed of subwavelength meta-atoms in a periodic or aperiodic manner, have received significant attention in recent decades because of their powerful ability to directly and locally manipulate wavefronts of electromagnetic (EM) waves [1–15]. Specifically, by engineering the meta-atoms with different resonant or non-resonant responses, the amplitude, phase, polarization at different frequency of EM waves can be tailored at will within sub-wavelength thickness. As such, the vigorously developed metasurfaces provide a versatile and flexible platform for high-density EM integration [16–18] to meet the increasing demands on the speed and memory of EM devices in modern science and technology. More importantly, metasurfaces are ideal candidates to integrate multiple diversified functionalities into single devices with deep-subwavelength thickness and high efficiencies. Among all the multi-functional metasurfaces, polarization has been widely used since polarization is uncorrelated with the other intrinsic properties of EM waves (e.g., amplitude, phase, and frequency) and thus can extend the information channels. For example, based on anisotropic meta-atoms with polarization-sensitive EM responses, various linear-polarization-multiplexed meta-devices were realized at different frequencies, exhibiting multiple functionalities triggered by incident EM waves with different linear polarizations [19–23]. In addition to linear polarization states, circular polarization states or spins of EM waves have been commonly exploited as another degree of freedom to design multi-functional metadevices based on the Pancharatnam–Berry (PB) phase mechanism achieved with spatially-varied meta-atoms [24–30]. Despite remarkable achievements with PB metasurfaces, the functionalities for right circularly polarized (RCP) and left circularly polarized (LCP) beams are often locked or mirrored since the PB phase has intrinsically opposite signs for two spins. For example, PB metasurfaces can only realize free-space beam steering into symmetric directions [31,32], surface plasmon polariton (SPP) excitation to opposite directions [33–35],

Received March 17, 2021; accepted May 6, 2021

E-mails: tangshiwei@nbu.edu.cn (S. Tang), feid@mci.sdu.dk (F. Ding)

and vortex beam generation with opposite topological charges [36–38].

To extend the functionalities, a commonly applied scheme is to merge several different PB metasurfaces in a compact configuration, each exhibiting a certain functionality as the incident circularly polarized (CP) light takes a particular spin [27,30]. However, this merging method has intrinsic constraints, such as low efficiency and cross-talks, limiting practical applications. Very recently, the spin-locked limitation of PB metasurfaces has been released by combining the orientation-dependent geometric phase and the dimension-dependent propagation phase, thereby providing a general and practical guideline toward the realization of spin-decoupled functionalities with a single metasurface for orthogonal circular polarization states [25,39]. Based on this approach, various spin-decoupled multi-functional metasurfaces have been realized, such as spin-multiplexing holograms [25,40], arbitrary spin-to-orbital momentum converters [14,41], spin-decoupled multifocal metalenses [42–44], and spin-decoupled wavefront shaping and polarization conversion [45,46].

In this paper, we present a concise review of the spin-decoupled metasurfaces. We start by introducing the fundamentals of PB phase metasurfaces. We then briefly summarize a class of multi-functional PB meta-devices based on the "merging" concept for CP waves. After that, we present the spin-decoupled meta-devices by combining the geometric phase and the propagation phase. Finally, we conclude this review with a short conclusion and personal outlook on the future directions of this rapidly growing research area.

2 Pancharatnam–Berry (PB) phase metasurfaces

2.1 Fundamental of PB phase

We first briefly introduce the physics of the PB phase. As early as 1956, Prof. Pancharatnam noted that the spin-reversed scattering-wave can gain an additional phase factor when the planar resonator is rotated by an angle of θ concerning the z-axis [47]. Such an additional phase, later interpreted as a geometric phase by Prof. Berry in Ref. [48], exactly equals to half of the solid angle of the area surrounded by two different traces connecting south and north poles on the Poincaré sphere (Fig. 1) [49], representing the two spin-reversed scattering processes on two resonators. Thus, the PB phase, dictated solely by the spin state of input light and the orientation angle of the scatter, exhibits the attractive dispersionless feature, which is different from that of the resonance-induced counterpart.

The easiest way to reveal the relationship between PB phase and rotation angle is to use the Jones calculus

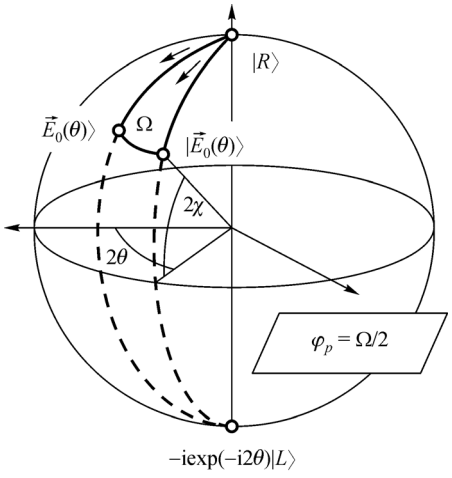

Fig. 1 Illustration of the Poincaré sphere. Reprinted with permission [49]. Copyright 2002, Optics Letter

[50,51]. In general, the Jones matrix of an anisotropic scatterer can be written as [52]

$$\begin{bmatrix} E_x^{\mathrm{o}} \\ E_y^{\mathrm{o}} \end{bmatrix} = \boldsymbol{R}(-\theta) \begin{pmatrix} \mathrm{e}^{\mathrm{i}\phi_x} & 0 \\ 0 & \mathrm{e}^{\mathrm{i}\phi_y} \end{pmatrix} \boldsymbol{R}(\theta) \begin{bmatrix} E_x^{\mathrm{i}} \\ E_y^{\mathrm{i}} \end{bmatrix}. \tag{1}$$

Here E_x^{i} and E_y^{i} represent the x- and y-components of the input electric fields, respectively. E_x^{o} and E_y^{o} are the x- and y-components of the output electric fields, respectively. θ is the rotation angle of the meta-atom relative to the reference coordinate system. R is a 2×2 rotation matrix that can be used for electric field transformation in the different reference systems. ϕ_x and ϕ_y represent the phase delays of the meta-atom for polarized light along the x- and y-axes, respectively. Notably, the transmission matrix can be expressed as follows:

$$\boldsymbol{M}(x,y) = \boldsymbol{R}(-\theta) \begin{pmatrix} \mathrm{e}^{\mathrm{i}\phi_x} & 0 \\ 0 & \mathrm{e}^{\mathrm{i}\phi_y} \end{pmatrix} \boldsymbol{R}(\theta). \tag{2}$$

Additionally, to independently manipulate the phase of the arbitrary orthogonal polarization states, the transmission matrix of the metasurface should satisfy [14,25]:

$$\begin{cases} M(x,y)|\kappa^+\rangle = \mathrm{e}^{\mathrm{i}\phi^+(x,y)}|\kappa^+\rangle^*, \\ M(x,y)|\kappa^-\rangle = \mathrm{e}^{\mathrm{i}\phi^-(x,y)}|\kappa^-\rangle^*, \end{cases} \tag{3}$$

where $|\kappa^+\rangle = \begin{bmatrix} \kappa_1^+ \\ \kappa_2^+ \end{bmatrix}$ and $|\kappa^-\rangle = \begin{bmatrix} \kappa_1^- \\ \kappa_2^- \end{bmatrix}$ represent two arbitrary orthogonal polarization states, and $\phi^+(x,y)$ and $\phi^-(x,y)$ are the corresponding modulated phase, where * denotes the complex conjugate. Hence, the transmission matrix $\boldsymbol{M}(x,y)$ can be reformulated as follows:

$$\boldsymbol{M}(x,y)=\begin{bmatrix} e^{i\phi^{+}(x,y)}\left(\kappa_1^{+}\right)^{*} & e^{i\phi^{-}(x,y)}\left(\kappa_1^{-}\right)^{*} \\ e^{i\phi^{+}(x,y)}\left(\kappa_2^{+}\right)^{*} & e^{i\phi^{-}(x,y)}\left(\kappa_2^{-}\right)^{*} \end{bmatrix}\begin{bmatrix} \kappa_1^{+} & \kappa_1^{-} \\ \kappa_2^{+} & \kappa_2^{-} \end{bmatrix}^{-1}. \tag{4}$$

If the incident light is circularly polarized, $|\kappa^{+}\rangle$ and $|\kappa^{-}\rangle$ are denoted as $\begin{bmatrix}1\\ i\end{bmatrix}$ and $\begin{bmatrix}1\\ -i\end{bmatrix}$, respectively. Combining Eqs. (2) and (4), the relationship between the modulated phase and the characteristics of the local field can be obtained as follows:

$$\begin{cases} |\phi_x-\phi_y|=\pi, \\ \phi^{+}(x,y)=\phi_x+2\theta, \\ \phi^{-}(x,y)=\phi_x-2\theta. \end{cases} \tag{5}$$

According to this equation, the desired phase delays ϕ_x, ϕ_y and the rotation angle θ at any position of the metasurface can be quickly solved. The modulation phase is determined by ϕ_x and 2θ. The propagation phase ϕ_x is mainly related to the material refractive index and the geometry of the meta-atom of the metasurface, and the PB phase 2θ is only determined by the rotation angle of the meta-atom. Note that the modulation phases $\phi^{+}(x,y)$ and $\phi^{-}(x,y)$ are the linear combinations of ϕ_x and 2θ. When passing through the meta-atom, the LCP and RCP light beams are transformed into their orthogonal polarization states, and they obtain the same propagation phase and an opposite PB phase. Through the linear combination of the propagation and PB phases, the independent phase control of the LCP and RCP light is achieved.

2.2 Applications of PB phase metasurfaces

PB metasurfaces have received widespread attention because of their powerful control capabilities for CP waves in different frequency domains while maintaining advantages of compactness, surface-confined configurations, multiple functionalities, and high efficiency, distinct from traditional devices based on natural metamaterials, which usually have the disadvantages of being bulky and inefficient. Capitalizing on the principle of the PB phase, numerous planar optical devices have been proposed and demonstrated, such as EM wave deflectors [53,54], planar imaging lenses [55,56], orbital angular momentum (OAM) generators [57–64], and SPP couplers [65,66].

One of the most fascinating EM wave manipulation effects based on PB metasurface is the photonic spin Hall effect (PSHE). PSHE has recently received widespread attention, but most of the mechanisms require huge systems and are very inefficient. In 2011, Hasman's team demonstrated a plasmonic device that can compactly realize PSHE. The device is constructed by milling a 200-nm-thick gold film with a collection of nanopores distributed in a curve, whose orientations are spatially varied with θ [67]. Their results are not only based on the anisotropy caused by coupling but also directly use nanopores with anisotropic shapes to generate the PB phase they need (Fig. 2(a)). In 2012, Huang et al. experimentally realized a plasmonic metasurface that exhibits switchable anomalous refraction for CP waves [53]. As the abrupt phase change is independent of the resonance feature of the constituent plasmonic antennas, the metasurface exhibits broadband operation with dispersionless phase discontinuities (Fig. 2(b)).

To improve the efficiency of the PB metasurface, Luo et al. realized PSHE with an efficiency of about 100% with deep sub-wavelength metasurfaces composed of metal-insulator-metal (MIM) meta-atoms in the microwave range, as shown in Fig. 2(c). The strict analysis is carried out through the Jones matrix, and the basic criteria for realizing 100% efficiency PSHE metasurface are established [31]. For the visible light, Zheng et al. designed a geometric metasurface hologram working in reflection based on MIM meta-atoms that function as broadband and highly efficient half-wave plates (HWPs) [68]. At λ = 825 nm, its diffraction efficiency can reach as high as 80%. At the same time, it has a wide operation bandwidth between 630 and 1050 nm. In this case, the 16-level phase distribution has been effectively and precisely controlled by tailoring the orientation of the corresponding meta-atoms. Since the designed metasurface has an ultra-thin and uniform thickness (only 30 nm), it can be compatible with scalar diffraction theory even at sub-wavelength pixel sizes, thus simplifying the design of holograms. This technology has been flexibly applied to optical security, laser beam shaping, and other fields (Fig. 2(d)).

Besides high-efficiency reflective PB phase metasurfaces, the PB phase has been extended to realize efficient transmissive metasurfaces. As shown in Fig. 2(e), Zhou's research group showed that 100% efficient PSHE can be achieved in the lossless transmission PB metasurface [69]. They used the Jones matrix and effective current analysis to make a preliminary understanding and design the corresponding meta-atoms in this work. After the design, they manufactured a microwave PB metasurface and consequently proved that its PSHE efficiency can be as high as 91% through experiments. The microwave metasurface they built is based on a three-layered structure, whose total thickness is much smaller than the wavelength. This research promotes the development of PB metadevices with higher efficiency and performance in the transmission mode.

However, the high intrinsic losses of the plasmonic materials in the visible range (e.g., 400 to 700 nm) have prevented the realization of highly efficient metasurfaces in this region, which can be partially overcome by using high refractive index dielectric materials with a transparency window in the visible spectrum, such as titanium dioxide (TiO_2), gallium nitride (GaN), and silicon nitride (Si_3N_4).

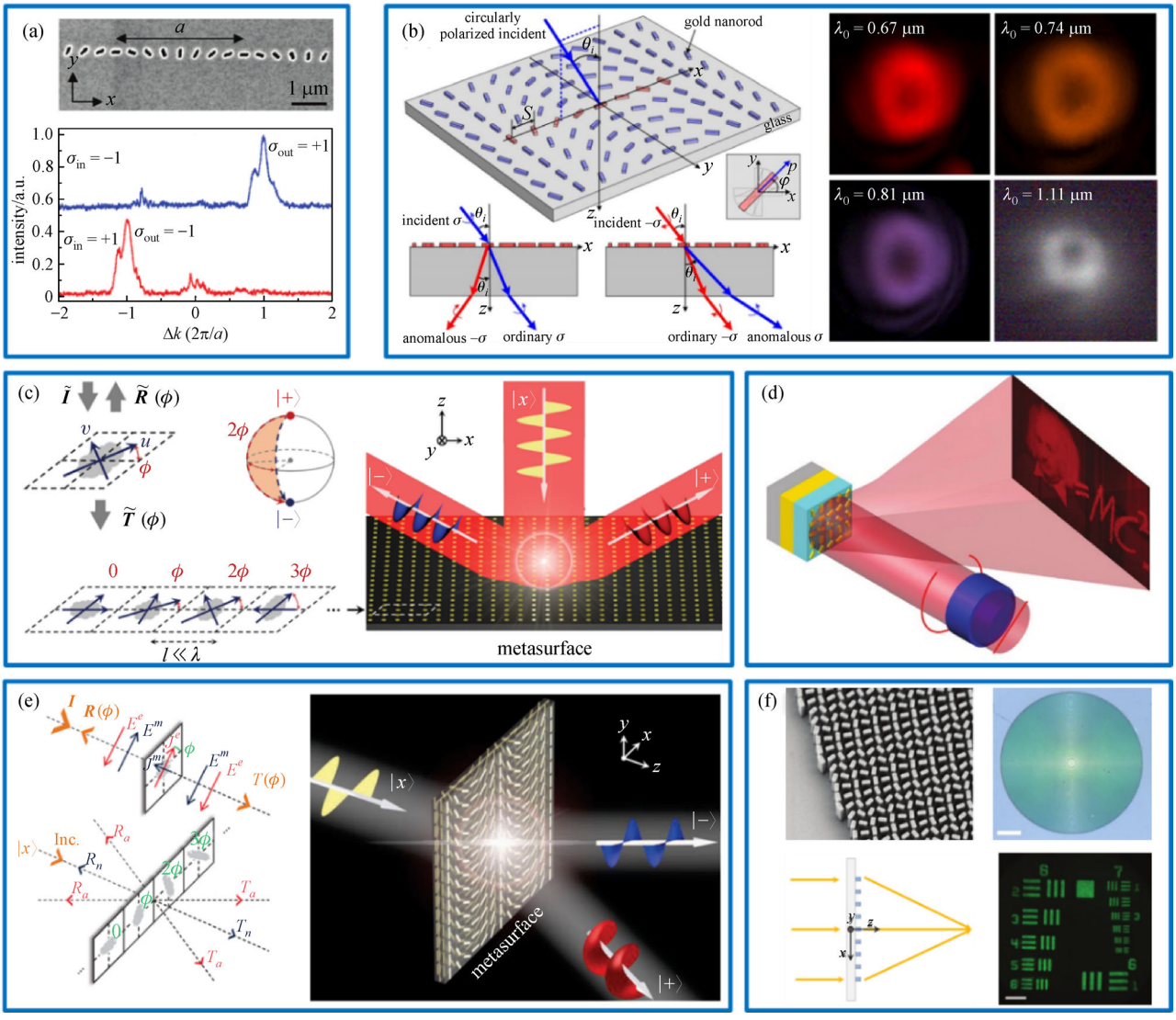

Fig. 2 (a) PSHE in the plasmon chain. Scanning electron microscope (SEM) images of the surfaces of the plasmons and spin-dependent momentum deviation of a metasurface. (b) Images and schematic illustrations of a refract dipole array, where the broadband anomalous refraction can be observed ranging from visible to near-infrared wavelengths. (c) Schematic diagram of achieving 100% efficiency PSHE on the reflective metasurface: the specular reflection mode disappears completely, and when linearly polarized light is incident, it will be split into two spin-polarized reflected beams that propagate in the directions of two illegal lines. (d) The circularly polarized incident beam is based on the illustration of the computer-generated hologram reflecting the nanorods. The linearly polarized beam passes through the quarter-wave plate and is converted into a circularly polarized incident beam. On the metasurface, the reflected beam forms a holographic image in the far-field. (e) Schematic diagram of 100% efficiency PSHE achieved by PB metasurfaces that meet the conditions in the transmission geometry. (f) Optical image of the metalens designed at the wavelength of 660 nm, the SEM micrograph of the fabricated metalens, and the image formed by the metalens in the transmission geometry. (a) Reprinted with permission [67]. Copyright 2011, Nano Letters. (b) Reprinted with permission [53]. Copyright 2012, Nano Letters. (c) Reprinted with permission [31]. Copyright 2015, Advanced Optical Materials. (d) Reprinted with permission [68]. Copyright 2015, Nature Nanotechnology. (e) Reprinted with permission [69]. Copyright 2017, Physical Review Applied. (f) Reprinted with permission [4]. Copyright 2016, Science

In 2016, Capasso's team demonstrated the high-aspect-ratio TiO_2 metasurfaces, which can be fabricated and designed as metalenses with NA = 0.8 [4]. Diffraction-limited focusing has been successfully implemented at wavelengths of 405, 532, and 660 nm with corresponding efficiencies of 86%, 73%, and 66%, respectively. The metalenses can resolve nanoscale features separated by subwavelength distances and provide a magnification as high as 170×, with image qualities comparable to a state-of-the-art commercial objective.

3 Spin-decoupled metasurfaces based on "merging" concept

As mentioned above, PB metasurfaces can arbitrarily control the response of electromagnetic waves, thereby realizing various electromagnetic wave manipulation functions. Facing the increasing demands on data-storage capacity and information processing speed in modern science and technology, electromagnetic integration plays an increasingly important role, which has intrigued intensive attention with remarkable applications. A goal pursued by scientists and engineers along this development is to make miniaturized devices as small as possible yet equipped with powerful functionalities as many as possible. A simple scheme developed in the early years utilized the so-called "merged" meta-structures to design multi-functional metasurfaces. In such a scheme, people first designed the individual metasurfaces exhibiting their functions and then construct a multi-functional device simply by merging the two structures. Below we present several examples to illustrate how the scheme works.

In 2015, Luo et al. proved that the reflective PB metasurface could be used as an efficient broadband polarization detector [31]. PB metasurfaces can efficiently reflect two spin components of input wave with unknown polarization to two different directions. Measuring the amplitudes and phases of these two anomalous reflection modes simultaneously, the original polarization state of the impinging wave can be retrieved. Similarly, on parallel lines, Pors et al. proposed the design and implementation of three birefringent blazed gratings based on the phase gradient metasurface in the reflection, which split orthogonal polarizations of different bases [70]. When at a wavelength of 800 nm, the relative diffraction contrast is equal to Stokes parameter of incident light (Fig. 3(a)).

Recently, Hasman's group experimentally demonstrated that the alliance of spin-enabled geometric phase and shared-aperture concepts can open a new pathway to implement photonic spin-controlled multi-functional metasurfaces [29,36,37]. Helicity-controlled multiple wavefronts such as vortex beams carrying different OAMs were demonstrated in the visible regime (780 nm), as shown in Fig. 3(b) [36]. They also combined the peculiar ability of random patterns to support an extraordinary information capacity and the polarization helicity control in the geometric phase mechanism, simply implemented in a two-dimensional structured matter by imprinting optical antenna patterns [37]. By manipulating the local orientations of the nanoantennas, multiple wavefronts with different functionalities via mixed random antenna groups can be generated, where each group controls a different phase function (Fig. 3(c)).

As shown in Fig. 3(d), two different holograms corresponding to LCP incident light and RCP incident light are calculated by the Gerchberg-Saxton algorithm, and then encoded in the MIM structural metasurfaces after superimposition [71]. Identical silver nanorods with different orientation angles can provide nearly continuous 16-level phase profiles over the entire 2π range and provide uniform reflection amplitude by eliminating the unintended amplitude variations caused by the different sizes of the nanorods. The holograms exhibit an efficiency of 59.2% at 860 nm and over 40% over 475–1100 nm. Two reconstructed images, a flower, and a bee exhibit helicity-dependent behavior. In the computer-generated hologram, the phase shift method is used to stagger the reconstructed images.

Figure 3(e) presents an optical bifunctional metasurface that can realize a hologram image or a vortex beam, depending on the helicity of excitation light [72]. To achieve their end, the authors first design two individual metasurfaces (both utilizing the metal-bar structure as basic meta-atoms), realizing one of the needed functionalities when they are shined by incident light taking CP with different helicities. The PB principle creates the desired phase profiles on two metasurfaces through rotating the metallic bars at different positions by appropriate angles. Since the two metasurfaces exhibit identical periodic structures and there are enough open spaces between metallic bars, the authors then merge two metasurfaces to obtain the final design in which all metallic bars do not touch with each other. Such a device was finally fabricated out and experimentally characterized, showing excellent bifunctional performances. However, the working efficiency of the device is relatively low, which is found to be around 9%.

Although the multi-functional metasurfaces can be realized by "merged" meta-structures mentioned above, the metadevices also have locked and mirrored functionalities for the RCP and LCP beams, which limits the practical applications. Wen et al. proposed a metasurface with an interleaved design to realize two distinct functionalities under LCP and RCP illumination respectively [30]. The proposed metasurface combines two different metasurfaces with different optical functionalities, as shown in Fig. 3(f). For LCP illumination, the RCP wave emitting from the first metasurface reconstructs a holographic image of "cat" while the RCP wave from the second metasurface diverges and forms a subtle background. For RCP illumination, the LCP wave emitting from the second metasurface focuses on a spot while the LCP wave from the first metasurface diverges. Thus, this merged metasurface functions as a hologram and a convex lens for LCP and RCP illumination, respectively. Using the same design principle, Zhang et al. realized a light sword metasurface lens with a helicity-dependent focal segment [73]. Chen et al. proposed a kind of metalens comprised of three regions with different phase profiles [74]. Every region can be considered as a helicity-dependent sub-metalens, and these three sublenses have the same axis and different focal lengths. Thus, the proposed metasurface can

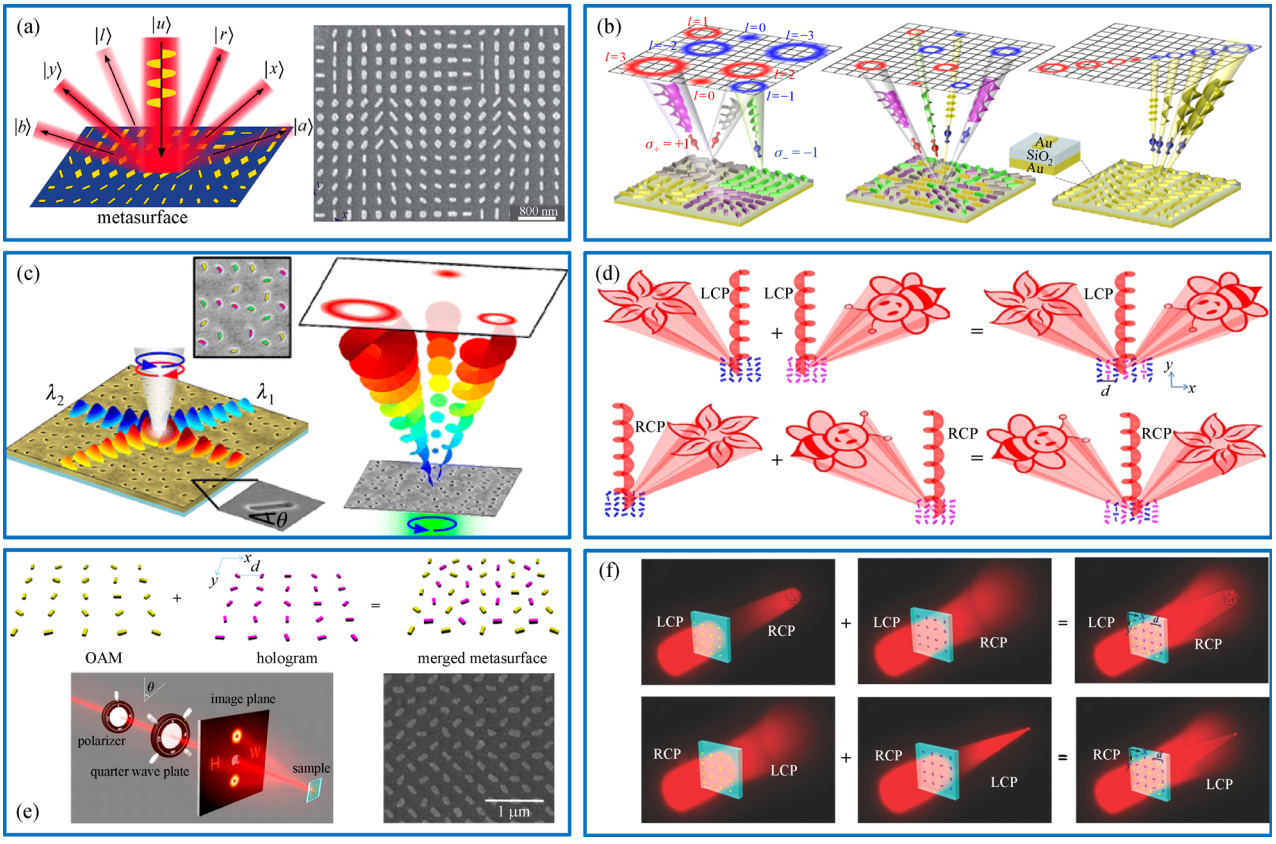

Fig. 3 Multi-functional devices designed with merged structures. (a) Illustration of the working principle. The state of the beam polarization can be detected without multiple measurements or an interferometric setup. (b) Schematic far-field intensity distribution of wavefronts with positive (red) and negative (blue) helicities emerging from segmented, interleaved, and harmonic response geometric phase metasurfaces composed of gap-plasmon nanoantennas (inset). Here, l denotes the topological charge of the spin-dependent OAM wavefronts. (c) Near-field open channels via disordered gradient metasurfaces. Schematic of directional SPP channels opened by a DGM. The scanning electron microscope image shows the 10 μm × 10 μm metasurface, wherein $r_{min} = 300$ nm and $d \approx 520$ nm, fabricated using a focused ion beam. The array consists of 80 nm×200 nm nanoantennas etched to a depth of 100 nm into a 200 nm thick gold film, evaporated onto a glass substrate. The diameter and width of the surrounding annular slit are 150 μm and 150 nm, respectively. (d) A metasurface that can generate multiple hologram images as shined by circularly polarized light with different helicity. (e) Design strategy, sample pictures, and experimental characterizations of a multi-functional metasurface that can generate holographic images or a vortex beam depending on the helicity of incident circularly polarized light. (f) Schematic of a metasurface with the interleaved design for helicity-dependent focusing and holograms. (a) Reprinted with permission [70]. Copyright 2015, Optica. (b) Reprinted with permission [36]. Copyright 2016, Science. (c) Reprinted with permission [37]. Copyright 2015, ACS Photonics. (d) Reprinted with permission [71]. Copyright 2015, Nature Communications. (e) Reprinted with permission [72]. Copyright 2017, ACS Photonics. (f) Reprinted with permission [30]. Copyright 2016, Advanced Optical Materials

focus LCP and RCP illumination into different spots.

In reviewing these meta-devices based on the "merging" concept, we find that the proposed design strategy is physically transparent and easy to implement. However, to make the "merging" process work, the adopted meta-atoms must be quite simple structures (say, metal bar) to avoid metallic overlapping. Unfortunately, these meta-atoms typically do not satisfy the 100%-efficiency criterion established for PB metasurfaces, and thus one type of meta-atoms can generate background noises in addition to the desired functionalities. As a result, such meta-devices typically suffer from the issues of low operating efficiencies and functionality cross-talking.

4 Spin-decoupled metasurface based on the combined phases

Although the integration of multiple functions can be realized with the "merging" concept, the spin-locked limitations of the PB metasurfaces still exist, thereby resulting in low efficiencies and intrinsic cross-talk. Recently, the spin-locked limitation of PB metasurfaces has been released by combining the orientation-dependent geometric phase and the dimension-dependent propagation phase, providing a general and practical guideline toward the realization of spin-decoupled functionalities with a single metasurface for orthogonal circular polarization

[25,39]. Based on this approach, various spin-decoupled multi-functional metasurfaces have been realized, such as spin-multiplexing holograms [25,40], arbitrary spin-to-orbital momentum converters [14], spin-decoupled multi-focal metalenses [42–44], and spin-decoupled wavefront shaping and polarization conversion [45,46].

By combining the geometric phase and the propagation phase of the reflected fields, spin-decoupled multi-functional metasurfaces have been demonstrated in reflection. In 2020, Xu et al. reported a strategy for achieving large-capacity multi-functional metasurface spin decoupling by reusing frequency and wave vector degrees of freedom, as shown in Fig. 4(a) [75]. To achieve the inherent limitation of the completely decoupled spin flipping PB phase between the two states, the researchers integrated the propagation phase and the geometric phase in an open-loop resonator and a crossbar in a checkerboard configuration. Decoupled or unlocking two spins by combining geometric phase and propagation phase is proposed as a new method [45,76,77]. Xu et al. proposed a concept of triple information multiplexer multitasking to prevent the limited system capacity. The triple information is rotation, wave vector, and frequency. Composite meta-atoms with crossbar and double gap SRRs were designed. It is characterized by a thin profile of $\lambda_0/8$ even at high frequencies, and the crosstalk of modes and spins can be ignored. A kaleidoscope overclocker was designed to verify the feasibility of three-degree-of-freedom multiplexing, which was performed at two microwave frequencies. This research is carried out in the case of reflection, and this discovery can be extended to transmission geometries at multiple frequencies and other efficient achromatic devices. In 2019, Xu et al. demonstrated another kind of spin-decoupled metasurfaces, which shows the advanced property of independent wavefront control [45]. By applying the geometric phase and propagation phase of the heterogeneous and anisotropic metasurfaces, modulation can be performed separately. To combine CP versatility and extreme wavefront control in a single planar device with high work efficiency, the researchers used meta-atoms characterized by low linear polarization crosstalk. As shown in Fig. 4(b), the bifunctional device has been realized, which combines the functionalities of beam bending and focusing when the metasurface is illuminated by normally incident LCP and RCP waves. In 2019, Feng's group proposed a reflective dual-helicity decoupled coding metasurface to realize completely independent control of OAM vortices for two orthogonal

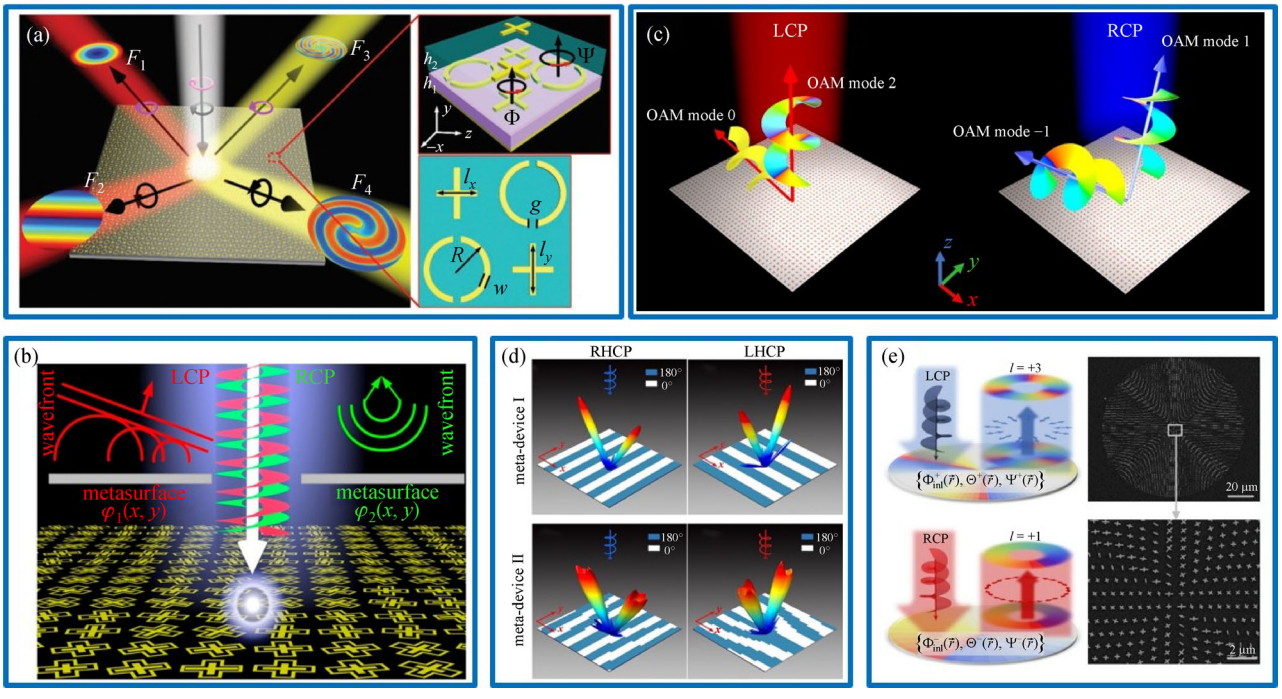

Fig. 4 (a) Schematic diagram of a four-port multiplexer using the proposed spin-decoupled meta-atom. (b) Illustration of two completely different wavefronts: oblique planar wavefront and a focusing wavefront. (c) Schematic of a bifunctional reflective metasurface dependent on the helicity. For the LCP incidence, the reflective beams are generated to have OAM modes $l = 2$ and $l = 0$. For RCP incidence, two vortex beams carrying OAM modes $l = 1$ and $l = -1$. (d) Schematic diagram of a meta-device designed to generate independent electromagnetic functions. (e) Left panel: schematics of light scatterings at a meta-device exhibiting vortex wavefront carrying different topological charges under illuminations of LCP and RCP incidences. Right panel: SEM images of the fabricated sample. (a) Reprinted with permission [75]. Copyright 2020, Advanced Materials Technologies. (b) Reprinted with permission [45]. Copyright 2019, ACS Photonics. (c) Reprinted with permission [15]. Copyright 2019, Physical Review Applied. (d) Reprinted with permission [76]. Copyright 2020, Annalen der Physik. (e) Reprinted with permission [84]. Copyright 2020, Nanophotonics

helicities, as shown in Fig. 4(c) [15]. The element combines both the propagation phase and geometric phase, thus overcoming the inherent limitation encountered by conventional geometric phase elements whose phase responses are constrained to be opposite values for different CP waves.

In 2020, Guo et al. proposed a new method for efficiently realizing independent spin control in an ultra-wideband using a spin-decoupled encoding metasurface (Fig. 4(d)) [76]. Combined with the Jones matrix, two HWPs with an intrinsic phase difference of 90° can form a 1-bit encoded metasurface, which can be used for manipulating orthogonal spins. They found a simple hybrid method, which is to rasterize when the propagation phase and geometry are the same. In this way, there can be several different meta-atoms functioning as efficient HWPs with different initial phases [77–80]. There, the operating bandwidth is broadened, and the complexity of the design is reduced because of the additional degrees of freedom. They used digital and coded metasurfaces with discrete phase elements to achieve multiple wave functions [81–83]. The researchers realized two ultra-wideband spin-decoupling meta-devices through the proposed coding elements: the first one can show different deflection angles for two spins. In contrast, the second one can create vortex beams with different topological charges when different spins are excited. The metasurface proposed here has the widest operating bandwidth for spin-decoupled wavefront control so far. It can be used in many areas, such as multi-functional low-scattering equipment in the microwave area and multi-channel metasurface antennas.

Very recently, Zhou's group established a generic strategy to design high-efficiency metadevices that create complex vectorial optical fields with desired wavefronts and polarization distributions (Fig. 4(e)) [84]. By exploring the full capabilities of meta-atoms in controlling light polarizations and combining two different mechanisms (propagation phases and PB phases) to generate phase shifts for incident light, they designed and fabricated two metadevices working at telecom wavelengths and experimentally demonstrate their bifunctional generations of two vectorial vortex beams possessing different topological charges and distinct polarization distributions.

The spin-decoupled metasurfaces mentioned above are mainly focused on molding propagating waves. Nevertheless, high-efficiency spin-decoupled manipulation of both propagating waves and surface waves remains so far largely unexplored. In 2020, Zhou's Group proposed a new strategy to realize meta-devices that can efficiently and simultaneously manipulate the wavefronts of propagating waves and surface waves in a predesigned manner, with functionalities dictated by the helicity of excitation CP wave [85]. They experimentally demonstrated two kinds of meta-devices in the microwave ranges, as shown in Fig. 5(a). One can convert an input CP propagating wave to a surface wave with a wavefront depending on the helicity of the excitation CP wave. The other microwave meta-device can realize either an anomalously deflected propagating wave or a focused surface wave, upon excitations of CP propagating waves with different helicities. In the same year, Zhou's group extended this concept and experimentally achieved a similar bifunctional metasurface in the terahertz band, shown in Fig. 5(b) [86].

In 2019, Yin et al. demonstrated a kind of terahertz spin-decoupled bifunctional meta-coupler, which can realize anomalous reflection for LCP waves and convert the incident waves into the surface wave for RCP waves, as shown in Fig. 5(c) [87]. But such work just stays in theoretical calculation. In 2020, Meng et al. designed the efficient spin-decoupled multi-functional Gap Surface Plasmon (GSP) gradient metasurfaces and experimentally demonstrated simultaneous spin-controlled unidirectional SPP excitation and anomalous beam steering in the optical regime under orthogonal RCP and LCP light incidence, respectively (top panel of Fig. 5(d)) [88]. The spin-decoupled GSP gradient metasurface, consisting of rotated GSP-based nanoscale HWPs, combines both resonance and PB phases to produce two different spin-dependent linear phase gradients, thereby enabling SPP excitation and anomalous reflection simultaneously at normal incidence (bottom panel of Fig. 5(d)). The proof-of-concept fabricated metasurface exhibits broadband (850–950 nm) operation featuring efficient ($>22\%$) unidirectional SPP excitation and high-efficiency (48% on average) anomalous beam steering for RCP and LCP incident light, respectively.

Compared to reflective devices, the spin-decoupled multi-functional metasurfaces in transmission geometry are more appealing to practical applications. In 2018, Cai et al. proposed a novel approach to design a new type of PB bifunctional metasurfaces with extremely high efficiencies in a single device by using multi-layered meta-atoms composed of metallic resonators and dielectric layers, which can operate in both transmission and reflection modes, relying on the incident chirality [89]. Due to the Lorentz reciprocal phenomenon in metasurfaces, the asymmetric transmission has been demonstrated theoretically and experimentally [90,91]. Asymmetric transmission effects can be realized by converting the incident polarization states, which provides a possibility to realize two different functions depending on the propagations of the incident waves on the metadevices. As a proof of concept, two kinds of meta-atoms under the framework of Jones matrices are designed. The former carries PB phases in both reflection and transmission schemes, while the transmission mode exhibits a reverse chirality compared with incident one. The latter keeps the handedness of incidence for RCP and LCP waves while carrying the PB phase only in the reflection scheme. Both metadevices exhibit high efficiencies within the range of $88\%-94\%$ (Fig. 6(a)). In 2020, Ding et al. proposed a transmissive metasurface based on multi-layered cascaded

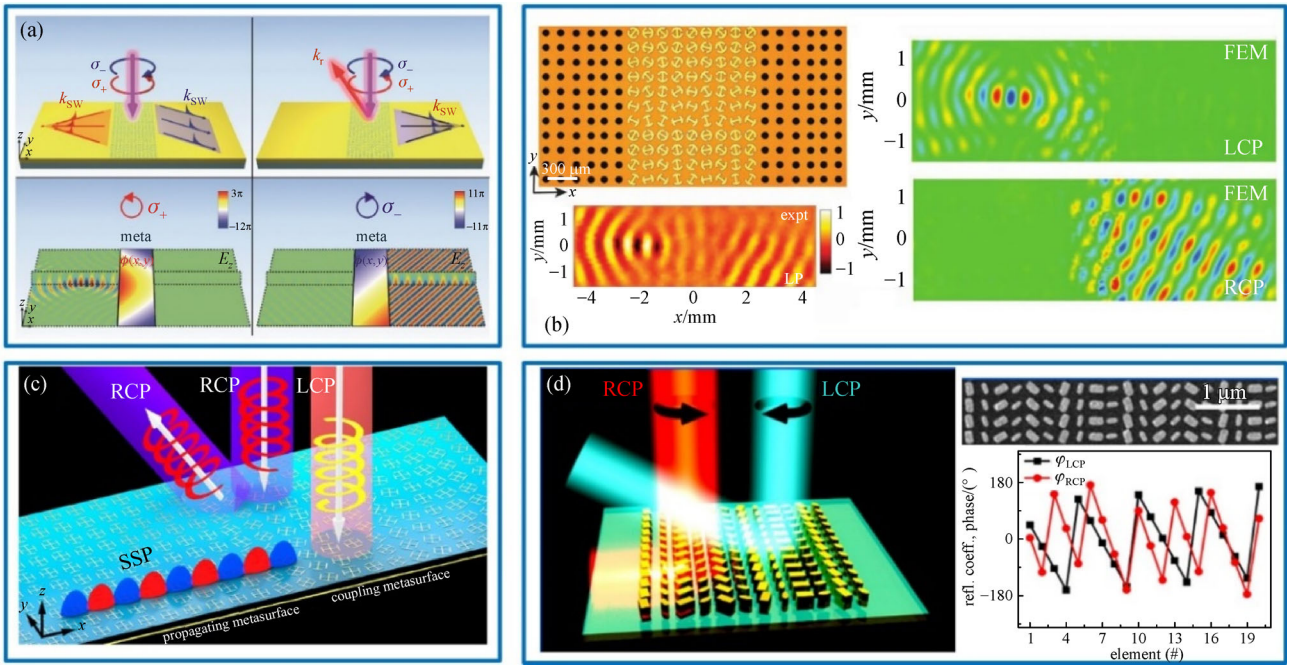

Fig. 5 (a) Schematics of the proposed metasurfaces to achieve helicity-delinked manipulations on both propagating wave and surface waves, which can convert incident CP waves of opposite helicity to surface waves possessing different wavefronts and traveling to opposite directions, both exhibiting extremely high efficiencies. Numerically computed $Re[E_z]$ field patterns on the surface of a plasmonic metal supporting a surface wave mode with an eigen wavevector are placed on the top surface of the plasmonic metal. Color maps show the phase distributions. (b) Picture of part of the fabricated sample consisting of a PB meta-device connected with two artificial metals. Simulated and measured near field pattern on a plane 50 μm underneath the sample. (c) Schematic view of the bifunctional meta-coupler that can realize circular polarization controlled unidirectional SSP excitation and anomalous reflection. (d) Left panel: schematic of the spin decoupled multi-functional GSP gradient metasurface for unidirectional SPP coupling and anomalous beam steering under normally incident RCP and LCP light, respectively. Right panel: SEM images of the fabricated spin decoupled GSP gradient metasurface and the calculated reflection phase profiles of the spin decoupled GSP gradient metasurface under RCP (red dots) and LCP (black squares) incidence at 850 nm. (a) Reprinted with permission [85]. Copyright 2020, Nanophotonics. (b) Reprinted with permission [86]. Copyright 2020, Advanced Science. (c) Reprinted with permission [87]. Copyright 2019, Optics Express. (d) Reprinted with permission [88]. Copyright 2020, ACS Photonics

structures, which functionalities can be independently and arbitrarily designed for two orthogonal spin states. Geometric phase and propagation phase responses are combined to realize spin-decoupled phase tuning [92].

Even though the multi-layered meta-atoms could achieve high transmission for the spin-decoupled devices in the microwave range, it is almost impossible to be extended to the high-frequency range, such as the optical range, because of the complex transmission structure design and fabrication as well as the high absorption of metals. Therefore, all-dielectric spin-decoupled meta-devices have been proposed. In 2017, Mueller et al. proposed a new approach that combines PB and propagating phases to encode arbitrary phase profiles on any two orthogonal polarization states (linear, circular, or elliptical), and experimentally demonstrated chiral holograms based on transmissive TiO_2 metasurfaces, which can efficiently generate different far-field images for RCP and LCP excitations at λ = 532 nm (Fig. 6(b)) [25].

In 2020, Fan et al. proposed a new class of metasurface polarization optics, which enables the imposition of two arbitrary and independent amplitude profiles on any pair of orthogonal states of polarization [93]. In this research, by constructing a meta-atoms interference system and introducing two wavefront modulation mechanisms with propagation phase and geometric phase, the interaction between incident polarized light and the meta-atoms system is analyzed. Then the meta-atoms system can satisfy Jones Matrix. In this system, phase control plays an important role. It serves as a bridge to establish the relationship between polarization and amplitude. This work also proved a new class of optical devices, including chiral grayscale metasurface and chiral shadow rendering of structured light (Fig. 6(c)), which expands the scope of metasurface polarization optics, establishes the relationship between polarization and amplitude, opens a new path for multi-functional photonic integration.

In 2021, Chen et al. proposed a new route for the phase manipulation of metasurfaces based on the anisotropic dielectric nanoantennas with subwavelength height, modulating two orthogonal CP light phases independently (Fig. 6(d)) [94]. Different holograms are presented in high

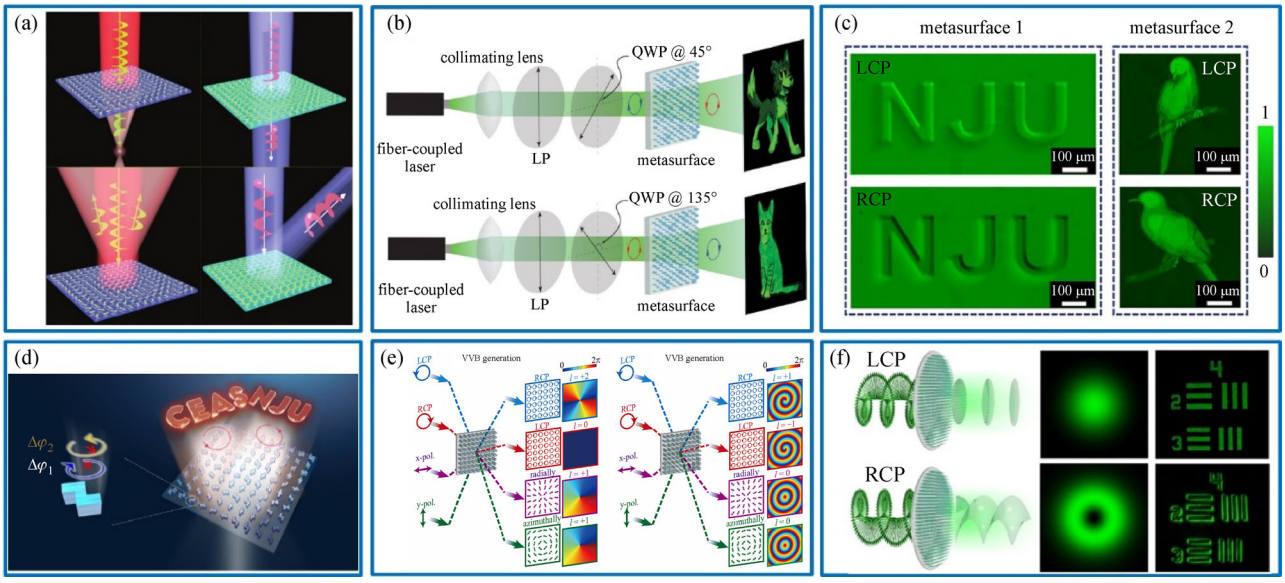

Fig. 6 Spin-decoupled metadevices. (a) Manipulating CP waves in desired multi-prescribed manners, especially in both transmission and reflection schemes, is of particular importance. Specially tailored PB meta-atoms with helicity-dependent transmissions and reflections are used to design high-efficiency CP bifunctional metasurfaces. Two kinds of bifunctional metadevices are designed and characterized at microwave frequencies, and both exhibit remarkably high efficiencies (88%–94%). (b) Experimental demonstration of chiral holograms realized with a single TiO_2 metasurface encoding two independent hologram phase profiles for LCP (dog) and RCP (cat) at λ = 532 nm. (c) Experimentally captured optical images of the metasurface nanoprinting illuminated with LCP and RCP light. (d) Spin-decoupled holograms with chiral meta-atoms. (e) Schematic of cylindrical vector beam generation in dielectric metasurfaces. (Left) vector vortex beam generation. (Right) vector Bessel beam generation. Each schematic contains four excitation cases marked by different colors. The color maps illustrate the corresponding phase distributions, where the number represents the value of the topological charge and the carrying OAM. (f) Spin-multiplexed optical imaging system. For a light incident on the device with LCP, the metasurface imprints a masking function on the output beam resulting in a constant phase profile and a Gaussian intensity distribution and flips the handedness of the incident polarization. For a light incident on the same device with RCP, the metasurface imprints another masking function, resulting in a spiral phase profile and a donut-shaped intensity distribution, and again flips the handedness of the polarization. (a) Reprinted with permission [89]. Copyright 2018, Annalen der Physik. (b) Reprinted with permission [25]. Copyright 2017, Physical Review Letters. (c) Reprinted with permission [93]. Copyright 2020, Physical Review Letters. (d) Reprinted with permission [94]. Copyright 2021, Nano Letters. (e) Reprinted with permission [95]. Copyright 2020, Nanophotonics. (f) Reprinted with permission [96]. Copyright 2020, Nano Letters

performances as the spin switched.

In 2020, Xu et al. proposed a general method for generating cylindrical vector beams in the terahertz range, which utilizes all-dielectric metasurfaces (Fig. 6(e)) [95]. Two circularly polarized output beams in cross-polarization are generated under circularly polarized incidence, and the two beams are superimposed with each other to achieve multiple spatially distributed beams. They have realized two metasurface cylindrical vector beam generators, among which one is for generating vector vortex beams, and the other can produce vector Bessel beams under polarized incidence.

In 2020, Huo et al. proposed a spin-multiplexed optical imaging system incorporating an all-dielectric metasurface that can perform a two-dimensional spatial differentiation operation and achieve isotropic edge detection, which can be used for either diffraction-limited bright-field imaging or isotropic edge-enhanced phase-contrast imaging (Fig. 6(f)) [96].

5 Conclusion

In summary, we have presented a brief review of the developments of spin-decoupled PB metasurfaces. We first briefly introduced the mechanism of PB metasurface and then summarized a class of multi-functional PB meta-devices based on the “merging” concept for CP waves. After that, we present the spin-decoupled meta-devices by combining the geometric phase and the propagation phase and review such kinds of spin-decoupled metasurface from two aspects of transmission and reflection geometries. Before concluding this review, we would like to mention many promising research directions on spin decoupled PB metasurfaces, based on our perspectives. We take active and tunable spin decoupled PB metasurfaces/meta-devices as an example. So far, most of the polarization-encoded metasurfaces can only achieve passive and static functionalities. Thus, it is highly desired to make tunable spin decoupled PB meta-devices exhibiting actively tunable

manipulations on CP waves with fast switching speed, which is now an extremely popular topic in metasurface research.

Acknowledgements S. Tang acknowledges the support from the National Natural Science Foundation of China (Grant No. 11604167), and Zhejiang Province Natural Science Foundation of China (No. LY19A040004). F. Ding acknowledges the support from Villum Fonden (Nos. 00022988 and 37372).

References

1. Cai T, Wang G, Tang S, Xu H, Duan J, Guo H, Guan F, Sun S, He Q, Zhou L. High-efficiency and full-space manipulation of electromagnetic wave fronts with metasurfaces. Physical Review Applied, 2017, 8(3): 034033
2. Cai T, Tang S, Wang G, Xu H, Sun S, He Q, Zhou L. High-performance bifunctional metasurfaces in transmission and reflection geometries. Advanced Optical Materials, 2017, 5(2): 1600506
3. Díaz-Rubio A, Asadchy V S, Elsakka A, Tretyakov S A. From the generalized reflection law to the realization of perfect anomalous reflectors. Science Advances, 2017, 3(8): e1602714
4. Khorasaninejad M, Chen W T, Devlin R C, Oh J, Zhu A Y, Capasso F. Metalenses at visible wavelengths: Diffraction-limited focusing and subwavelength resolution imaging. Science, 2016, 352(6290): 1190–1194
5. Moreno G, Yakovlev A B, Bernety H M, Werner D H, Xin H, Monti A, Bilotti F, Alu A. Wideband elliptical metasurface cloaks in printed antenna technology. IEEE Transactions on Antennas and Propagation, 2018, 66(7): 3512–3525
6. Sima B, Chen K, Luo X, Zhao J, Feng Y. Combining frequency-selective scattering and specular reflection through phase-dispersion tailoring of a metasurface. Physical Review Applied, 2018, 10(6): 064043
7. Liu K, Guo W, Wang G, Li H, Liu G. A novel broadband bi-functional metasurface for vortex generation and simultaneous RCS reduction. IEEE Access: Practical Innovations, Open Solutions, 2018, 6: 63999–64007
8. Zhang Y, Liu W, Gao J, Yang X. Generating focused 3D perfect vortex beams by plasmonic metasurfaces. Advanced Optical Materials, 2018, 6(4): 1701228
9. Cai T, Wang G, Zhang X, Liang J, Zhuang Y, Liu D, Xu H. Ultra-thin polarization beam splitter using 2-D transmissive phase gradient metasurface. IEEE Transactions on Antennas and Propagation, 2015, 63(12): 5629–5636
10. Pfeiffer C, Zhang C, Ray V, Guo L J, Grbic A. High performance bianisotropic metasurfaces: asymmetric transmission of light. Physical Review Letters, 2014, 113(2): 023902
11. Ni X, Emani N K, Kildishev A V, Boltasseva A, Shalaev V M. Broadband light bending with plasmonic nanoantennas. Science, 2012, 335(6067): 427
12. Yu N, Genevet P, Kats M A, Aieta F, Tetienne J P, Capasso F, Gaburro Z. Light propagation with phase discontinuities: generalized laws of reflection and refraction. Science, 2011, 334(6054): 333–337
13. Akram M R, Mehmood M Q, Bai X, Jin R, Premaratne M, Zhu W. High efficiency ultrathin transmissive metasurfaces. Advanced Optical Materials, 2019, 7(11): 1801628
14. Devlin R C, Ambrosio A, Rubin N A, Mueller J P B, Capasso F. Arbitrary spin-to-orbital angular momentum conversion of light. Science, 2017, 358(6365): 896–901
15. Ding G, Chen K, Luo X, Zhao J, Jiang T, Feng Y. Dual-helicity decoupled coding metasurface for independent spin-to-orbital angular momentum conversion. Physical Review Applied, 2019, 11(4): 044043
16. Kildishev A V, Boltasseva A, Shalaev V M. Planar photonics with metasurfaces. Science, 2013, 339(6125): 1232009
17. Yu N, Capasso F. Flat optics with designer metasurfaces. Nature Materials, 2014, 13(2): 139–150
18. Lin D, Fan P, Hasman E, Brongersma M L. Dielectric gradient metasurface optical elements. Science, 2014, 345(6194): 298–302
19. Ding F, Deshpande R, Bozhevolnyi S I. Bifunctional gap-plasmon metasurfaces for visible light: polarization-controlled unidirectional surface plasmon excitation and beam steering at normal incidence. Light, Science & Applications, 2018, 7(4): 17178
20. Boroviks S, Deshpande R A, Mortensen N A, Bozhevolnyi S I. Multifunctional metamirror: polarization splitting and focusing. ACS Photonics, 2018, 5(5): 1648–1653
21. Xu H X, Tang S, Ling X, Luo W, Zhou L. Flexible control of highly-directive emissions based on bifunctional metasurfaces with low polarization cross-talking. Annalen der Physik, 2017, 529(5): 1700045
22. Xu H, Tang S, Wang G, Cai T, Huang W, He Q, Sun S, Zhou L. Multifunctional microstrip array combining a linear polarizer and focusing metasurface. IEEE Transactions on Antennas and Propagation, 2016, 64(8): 3676–3682
23. Liu S, Jun Cui T, Noor A, Tao Z, Zhang H C, Bai G, Yang Y, Yang Zhou X. Negative reflection and negative surface wave conversion from obliquely incident electromagnetic waves. Light, Science & Applications, 2018, 7(5): 18008
24. Huang L, Mühlenbernd H, Li X, Song X, Bai B, Wang Y, Zentgraf T. Broadband hybrid holographic multiplexing with geometric metasurfaces. Advanced Materials, 2015, 27(41): 6444–6449
25. Balthasar Mueller J P, Rubin N A, Devlin R C, Groever B, Capasso F. Metasurface polarization optics: independent phase control of arbitrary orthogonal states of polarization. Physical Review Letters, 2017, 118(11): 113901
26. Xiao S, Zhong F, Liu H, Zhu S, Li J. Flexible coherent control of plasmonic spin-Hall effect. Nature Communications, 2015, 6(1): 8360
27. Choudhury S, Guler U, Shaltout A, Shalaev V M, Kildishev A V, Boltasseva A. Pancharatnam–Berry phase manipulating metasurface for visible color hologram based on low loss silver thin film. Advanced Optical Materials, 2017, 5(10): 1700196
28. Wang S, Wang X, Kan Q, Ye J, Feng S, Sun W, Han P, Qu S, Zhang Y. Spin-selected focusing and imaging based on metasurface lens. Optics Express, 2015, 23(20): 26434–26441
29. Maguid E, Yulevich I, Yannai M, Kleiner V, Brongersma M L, Hasman E. Multifunctional interleaved geometric-phase dielectric metasurfaces. Light, Science & Applications, 2017, 6(8): e17027
30. Wen D, Chen S, Yue F, Chan K, Chen M, Ardron M, Li K F, Wong P W H, Cheah K W, Pun E Y B, Li G, Zhang S, Chen X. Metasurface

device with helicity-dependent functionality. Advanced Optical Materials, 2016, 4(2): 321–327
31. Luo W, Xiao S, He Q, Sun S, Zhou L. Photonic spin Hall effect with nearly 100% efficiency. Advanced Optical Materials, 2015, 3(8): 1102–1108
32. Khorasaninejad M, Crozier K B. Silicon nanofin grating as a miniature chirality-distinguishing beam-splitter. Nature Communications, 2014, 5(1): 5386
33. Huang L, Chen X, Bai B, Tan Q, Jin G, Zentgraf T, Zhang S. Helicity dependent directional surface plasmon polariton excitation using a metasurface with interfacial phase discontinuity. Light, Science & Applications, 2013, 2(3): e70
34. Jiang Q, Bao Y, Lin F, Zhu X, Zhang S, Fang Z. Spin-controlled integrated near-and far-field optical launcher. Advanced Functional Materials, 2018, 28(8): 1705503
35. Jin J, Li X, Guo Y, Pu M, Gao P, Ma X, Luo X. Polarization-controlled unidirectional excitation of surface plasmon polaritons utilizing catenary apertures. Nanoscale, 2019, 11(9): 3952–3957
36. Maguid E, Yulevich I, Veksler D, Kleiner V, Brongersma M L, Hasman E. Photonic spin-controlled multi-functional shared-aperture antenna array. Science, 2016, 352(6290): 1202–1206
37. Veksler D, Maguid E, Shitrit N, Ozeri D, Kleiner V, Hasman E. Multiple wavefront shaping by metasurface based on mixed random antenna groups. ACS Photonics, 2015, 2(5): 661–667
38. Mehmood M Q, Mei S, Hussain S, Huang K, Siew S Y, Zhang L, Zhang T, Ling X, Liu H, Teng J, Danner A, Zhang S, Qiu C W. Visible-frequency metasurface for structuring and spatially multiplexing optical vortices. Advanced Materials, 2016, 28(13): 2533–2539
39. Ding F, Wang Z, He S, Shalaev V M, Kildishev A V. Broadband high-efficiency half-wave plate: a supercell-based plasmonic metasurface approach. ACS Nano, 2015, 9(4): 4111–4119
40. Zhang C, Divitt S, Fan Q, Zhu W, Agrawal A, Lu Y, Xu T, Lezec H J. Low-loss metasurface optics down to the deep ultraviolet region. Light, Science & Applications, 2020, 9(1): 55
41. Yuan Y, Zhang K, Ratni B, Song Q, Ding X, Wu Q, Burokur S N, Genevet P. Independent phase modulation for quadruplex polarization channels enabled by chirality-assisted geometric-phase metasurfaces. Nature Communications, 2020, 11(1): 4186
42. Tian S, Guo H, Hu J, Zhuang S. Dielectric longitudinal bifocal metalens with adjustable intensity and high focusing efficiency. Optics Express, 2019, 27(2): 680–688
43. Jin R, Tang L, Li J, Wang J, Wang Q, Liu Y, Dong Z. Experimental demonstration of multidimensional and multi-functional metalenses based on photonic spin hall effect. ACS Photonics, 2020, 7(2): 512–518
44. Li X, Li S, Wang G, Lei Y, Hong Y, Zhang L, Zeng C, Wang L, Sun Q, Zhang W. Tunable doublet lens based on dielectric metasurface using phase-change material. Modern Physics Letters B, 2020, 34 (28): 2050313
45. Xu H, Han L, Li Y, Sun Y, Zhao J, Zhang S, Qiu C. Completely spin-decoupled dual-phase hybrid metasurfaces for arbitrary wavefront control. ACS Photonics, 2019, 6(1): 211–220
46. Fan Q, Zhu W, Liang Y, Huo P, Zhang C, Agrawal A, Huang K, Luo X, Lu Y, Qiu C, Lezec H J, Xu T. Broadband generation of photonic spin-controlled arbitrary accelerating light beams in the visible. Nano Letters, 2019, 19(2): 1158–1165
47. Pancharatnam S. Generalized theory of interference and its applications. In: Proceedings of the Indian Academy of Sciences-Section A. Beilin: Springer, 1956, 398–417
48. Berry M V. Quantal phase factors accompanying adiabatic changes. Proceedings of the Royal Society of London. Series A, Mathematical and Physical Sciences, 1802, 1984(392): 45–57
49. Bomzon Z, Biener G, Kleiner V, Hasman E. Space-variant Pancharatnam–Berry phase optical elements with computer-generated subwavelength gratings. Optics Letters, 2002, 27(13): 1141–1143
50. Menzel C, Rockstuhl C, Lederer F. Advanced Jones calculus for the classification of periodic metamaterials. Physical Review A, 2010, 82(5): 053811
51. Armitage N P. Constraints on Jones transmission matrices from time-reversal invariance and discrete spatial symmetries. Physical Review. B, 2014, 90(3): 035135
52. Arbabi A, Horie Y, Bagheri M, Faraon A. Dielectric metasurfaces for complete control of phase and polarization with subwavelength spatial resolution and high transmission. Nature Nanotechnology, 2015, 10(11): 937–943
53. Huang L, Chen X, Mühlenbernd H, Li G, Bai B, Tan Q, Jin G, Zentgraf T, Zhang S. Dispersionless phase discontinuities for controlling light propagation. Nano Letters, 2012, 12(11): 5750–5755
54. Xu H, Ma S, Ling X, Zhang X, Tang S, Cai T, Sun S, He Q, Zhou L. Deterministic approach to achieve broadband polarization-independent diffusive scatterings based on metasurfaces. ACS Photonics, 2018, 5(5): 1691–1702
55. Chen X, Huang L, Mühlenbernd H, Li G, Bai B, Tan Q, Jin G, Qiu C W, Zentgraf T, Zhang S. Reversible three-dimensional focusing of visible light with ultrathin plasmonic flat lens. Advanced Optical Materials, 2013, 1(7): 517–521
56. Zhao Z, Pu M, Gao H, Jin J, Li X, Ma X, Wang Y, Gao P, Luo X. Multispectral optical metasurfaces enabled by achromatic phase transition. Scientific Reports, 2015, 5(1): 15781
57. Yue F, Wen D, Zhang C, Gerardot B D, Wang W, Zhang S, Chen X. Multichannel polarization-controllable superpositions of orbital angular momentum states. Advanced Materials, 2017, 29(15): 1603838
58. Chen P, Ge S, Duan W, Wei B, Cui G, Hu W, Lu Y. Digitalized geometric phases for parallel optical spin and orbital angular momentum encoding. ACS Photonics, 2017, 4(6): 1333–1338
59. Wen D, Yue F, Liu W, Chen S, Chen X. Geometric metasurfaces for ultrathin optical devices. Advanced Optical Materials, 2018, 6(17): 1800348
60. Gao H, Li Y, Chen L, Jin J, Pu M, Li X, Gao P, Wang C, Luo X, Hong M. Quasi-Talbot effect of orbital angular momentum beams for generation of optical vortex arrays by multiplexing metasurface design. Nanoscale, 2018, 10(2): 666–671
61. Li Y, Li X, Chen L, Pu M, Jin J, Hong M, Luo X. Orbital angular momentum multiplexing and demultiplexing by a single metasurface. Advanced Optical Materials, 2017, 5(2): 1600502
62. Yang K, Pu M, Li X, Ma X, Luo J, Gao H, Luo X. Wavelength-selective orbital angular momentum generation based on a plasmonic metasurface. Nanoscale, 2016, 8(24): 12267–12271

63. Ma X, Pu M, Li X, Huang C, Wang Y, Pan W, Zhao B, Cui J, Wang C, Zhao Z, Luo X. A planar chiral meta-surface for optical vortex generation and focusing. Scientific Reports, 2015, 5(1): 10365
64. Ren H, Li X, Zhang Q, Gu M. On-chip noninterference angular momentum multiplexing of broadband light. Science, 2016, 352 (6287): 805–809
65. Lin J, Mueller J P, Wang Q, Yuan G, Antoniou N, Yuan X C, Capasso F. Polarization-controlled tunable directional coupling of surface plasmon polaritons. Science, 2013, 340(6130): 331–334
66. Duan J, Guo H, Dong S, Cai T, Luo W, Liang Z, He Q, Zhou L, Sun S. High-efficiency chirality-modulated spoof surface plasmon meta-coupler. Scientific Reports, 2017, 7(1): 1354
67. Shitrit N, Bretner I, Gorodetski Y, Kleiner V, Hasman E. Optical spin Hall effects in plasmonic chains. Nano Letters, 2011, 11(5): 2038–2042
68. Zheng G, Mühlenbernd H, Kenney M, Li G, Zentgraf T, Zhang S. Metasurface holograms reaching 80% efficiency. Nature Nanotechnology, 2015, 10(4): 308–312
69. Luo W, Sun S, Xu H, He Q, Zhou L. Transmissive ultrathin Pancharatnam–Berry metasurfaces with nearly 100% efficiency. Physical Review Applied, 2017, 7(4): 044033
70. Pors A, Nielsen M G, Bozhevolnyi S I. Plasmonic metagratings for simultaneous determination of Stokes parameters. Optica, 2015, 2 (8): 716–723
71. Wen D, Yue F, Li G, Zheng G, Chan K, Chen S, Chen M, Li K F, Wong P W H, Cheah K W, Pun E Y, Zhang S, Chen X. Helicity multiplexed broadband metasurface holograms. Nature Communications, 2015, 6(1): 8241
72. Zhang C, Yue F, Wen D, Chen M, Zhang Z, Wang W, Chen X. Multichannel metasurface for simultaneous control of holograms and twisted light beams. ACS Photonics, 2017, 4(8): 1906–1912
73. Zhang Z, Wen D, Zhang C, Chen M, Wang W, Chen S, Chen X. Multifunctional light sword metasurface lens. ACS Photonics, 2018, 5(5): 1794–1799
74. Chen X, Chen M, Mehmood M Q, Wen D, Yue F, Qiu C W, Zhang S. Longitudinal multifoci metalens for circularly polarized light. Advanced Optical Materials, 2015, 3(9): 1201–1206
75. Xu H X, Hu G, Jiang M, Tang S, Wang Y, Wang C, Huang Y, Ling X, Liu H, Zhou J. Wavevector and frequency multiplexing performed by a spin-decoupled multichannel metasurface. Advanced Materials Technologies, 2020, 5(1): 1900710
76. Guo W L, Wang G M, Luo X Y, Hou H S, Chen K, Feng Y. Ultrawideband spin-decoupled coding metasurface for independent dual-channel wavefront tailoring. Annalen der Physik, 2020, 532 (3): 1900472
77. Zi J, Xu Q, Wang Q, Tian C, Li Y, Zhang X, Han J, Zhang W. Antireflection-assisted all-dielectric terahertz metamaterial polarization converter. Applied Physics Letters, 2018, 113(10): 101104
78. Xu J, Li R, Qin J, Wang S, Han T. Ultra-broadband wide-angle linear polarization converter based on H-shaped metasurface. Optics Express, 2018, 26(16): 20913–20919
79. Hu S, Yang S, Liu Z, Li J, Gu C. Broadband cross-polarization conversion by symmetry-breaking ultrathin metasurfaces. Applied Physics Letters, 2017, 111(24): 241108
80. Borgese M, Costa F, Genovesi S, Monorchio A, Manara G. Optimal design of miniaturized reflecting metasurfaces for ultra-wideband and angularly stable polarization conversion. Scientific Reports, 2018, 8(1): 7651
81. Wu H, Liu S, Wan X, Zhang L, Wang D, Li L, Cui T J. Controlling energy radiations of electromagnetic waves via frequency coding metamaterials. Advancement of Science, 2017, 4(9): 1700098
82. Guan C, Wang Z, Ding X, Zhang K, Ratni B, Burokur S N, Jin M, Wu Q. Coding Huygens' metasurface for enhanced quality holographic imaging. Optics Express, 2019, 27(5): 7108–7119
83. Liu S, Zhang L, Yang Q L, Xu Q, Yang Y, Noor A, Zhang Q, Iqbal S, Wan X, Tian Z, Tang W X, Cheng Q, Han J G, Zhang W L, Cui T J. Frequency-dependent dual-functional coding metasurfaces at terahertz frequencies. Advanced Optical Materials, 2016, 4(12): 1965–1973
84. Wang D, Liu T, Zhou Y, Zheng X, Sun S, He Q, Zhou L. High-efficiency metadevices for bifunctional generations of vectorial optical fields. Nanophotonics, 2020, 10(1): 685–695
85. Li S, Wang Z, Dong S, Yi S, Guan F, Chen Y, Guo H, He Q, Zhou L, Sun S. Helicity-delinked manipulations on surface waves and propagating waves by metasurfaces. Nanophotonics, 2020, 9(10): 3473–3481
86. Wang Z, Li S, Zhang X, Feng X, Wang Q, Han J, He Q, Zhang W, Sun S, Zhou L. Excite spoof surface plasmons with tailored wavefronts using high-efficiency terahertz metasurfaces. Advanced Science, 2020, 7(19): 2000982
87. Yin L Z, Huang T J, Han F Y, Liu J Y, Wang D, Liu P K. High-efficiency terahertz spin-decoupled meta-coupler for spoof surface plasmon excitation and beam steering. Optics Express, 2019, 27 (13): 18928–18939
88. Meng C, Tang S, Ding F, Bozhevolnyi S I. Optical gap-surface plasmon metasurfaces for spin-controlled surface plasmon excitation and anomalous beam steering. ACS Photonics, 2020, 7(7): 1849–1856
89. Cai T, Wang G M, Xu H X, Tang S W, Li H, Liang J G, Zhuang Y Q. Bifunctional Pancharatnam–Berry metasurface with high-efficiency helicity-dependent transmissions and reflections. Annalen der Physik, 2018, 530(1): 1700321
90. Fedotov V A, Mladyonov P L, Prosvirnin S L, Rogacheva A V, Chen Y, Zheludev N I. Asymmetric propagation of electromagnetic waves through a planar chiral structure. Physical Review Letters, 2006, 97(16): 167401
91. Liu J, Li Z, Liu W, Cheng H, Chen S, Tian J. High-efficiency mutual dual-band asymmetric transmission of circularly polarized waves with few-layer anisotropic metasurfaces. Advanced Optical Materials, 2016, 4(12): 2028–2034
92. Ding G, Chen K, Qian G, Zhao J, Jiang T, Feng Y, Wang Z. Independent energy allocation of dual-helical multi-beams with spin-selective transmissive metasurface. Advanced Optical Materials, 2020, 8(16): 2000342
93. Fan Q, Liu M, Zhang C, Zhu W, Wang Y, Lin P, Yan F, Chen L, Lezec H J, Lu Y, Agrawal A, Xu T. Independent amplitude control of arbitrary orthogonal states of polarization via dielectric metasurfaces. Physical Review Letters, 2020, 125(26): 267402
94. Chen C, Gao S, Song W, Li H, Zhu S N, Li T. Metasurfaces with planar chiral meta-atoms for spin light manipulation. Nano Letters, 2021, 21(4): 1815–1821
95. Xu Y, Zhang H, Li Q, Zhang X, Xu Q, Zhang W, Hu C, Zhang X,

Han J, Zhang W. Generation of terahertz vector beams using dielectric metasurfaces via spin-decoupled phase control. Nanophotonics, 2020, 9(10): 3393–3402

96. Huo P, Zhang C, Zhu W, Liu M, Zhang S, Zhang S, Chen L, Lezec H J, Agrawal A, Lu Y, Xu T. Photonic spin-multiplexing metasurface for switchable spiral phase contrast imaging. Nano Letters, 2020, 20(4): 2791–2798

Yingcheng Qiu received his bachelor's degree from Wenzheng College of Soochow University, China, in 2019. Since 2019, he has been a master student in the School of Physics Science and Technology at Ningbo University, China. His fields of interest include metamaterials and metasurfaces.

Shiwei Tang received his Ph.D. degree in Physics Department of Fudan University, China, in 2014. He was a postdoctoral fellow in Materials Science Department of Fudan University from 2014 to 2015. He joined Ningbo University, China, in 2016 and was promoted to an Associate Professor in 2019. His current research interests include metamaterials/metasurfaces, microcavities, plasmonics, and nanophotonics. He has published over 60 papers in *Advanced Materials*, *Advanced Functional Materials*, *ACS Nano*, *Optics Express*, etc.

Tong Cai received his B.S. and Ph.D. degrees in Electrical Engineering from Air Force Engineering University, China, in 2012 and 2017, respectively. He was with Air Force Engineering University, where he became a Lecturer in 2017 and an associate professor in 2020. He has been a Post-Doctoral Researcher with Zhejiang University since 2019. His research interests include metamaterials, metasurfaces and their applications to novel antennas and multifunctional devices.

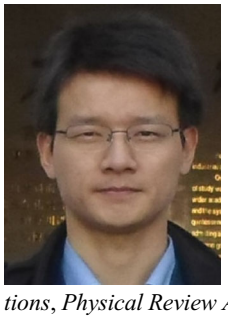

Hexiu Xu is a full Professor of Air Force Engineering University, China, since 2019. He has published more than 130 peer-reviewed journal papers in *Research*, *Nature Materials*, *Nature Photonics*, *Light*: *Science and Applications*, *Proceedings of IEEE*, *Advanced Materials*, *ACS Photonics*, *Photonics Research*, *IEEE Transaction on Antennas and Propagations*, *Physical Review Applied*, etc. He has also published 3 Chinese books, 1 English books and 2 English book chapters. He served as an editor of *AEU International Journal of Electronics and Communications* since 2014 and served as an invited reviewer for more than 20 leading journals. He has owned 28 China patents and has given more than 31 invited talks. He served as a special session chair 16 times in international conferences. His research interests include metamaterials/metasurfaces, and their applications to novel functional devices and microwave antennas. Dr. Xu received the 8th China Youth Science and Technology Innovation Award in 2013. He won the best Excellent Doctoral Dissertation Award at Air Force Engineering University in 2014 and later received the Excellent Doctoral Dissertation Award from Military, Shaanxi Province, and Chinese Institute of Electronics (CIE). He has hosted several programs such as the National Science Foundation of China, the Key Program of National Natural Science Foundation of Shaanxi Province, Natural Science Foundation of Shaanxi Province, China Scholarship Fund, and First-Class General and Special Financial Grant from China Postdoctoral Science Foundation. He receives five Young Scientist Awards like at URSI GASS, URSI AP-RASC, URSI EMTS, ACES and PIERs in 2019 and two First-class Technological Invention Awards from National Invention Association in 2019 and 2020, and four Scientific and Technological Progress Awards like Outstanding Award from Department of Education of Shaanxi government in 2021. He was awarded outstanding scientific and technological worker of CIE in 2018, a Young Talent from China Association for Science and Technology in 2017, Young Scientist Nova from Shaanxi Technology Committee in 2016. Dr. Xu is now also a Fellow of IET and a Senior Member of IEEE and CIE.

Fei Ding received his B.S. and Ph.D. degrees in Optical Engineering from Zhejiang University, China, in 2010 and 2015, respectively. He was a Postdoctoral Fellow at the Centre for Nano Optics at the University of Southern Denmark (SDU Nano Optics) in Denmark from 2015 to 2019. He is currently an assistant professor at SDU Nano Optics. His current research interests are in the areas of nanophotonics, applied electromagnetics, metasurfaces, plasmonics, and quantum nanophotonics, with a particular focus on innovative and extreme aspects of light-matter interaction at the nanoscale. He has authored or co-authored more than 50 peer-reviewed journal papers in *Reports on Progress in Physics*, *Light*: *Science & Applications*, *Nature Communications*, *Science Advances*, *Advanced Materials*, *ACS Nano*, *Nano Letters*, and *Laser & Photonics Reviews*, receiving more than 3500 citations (Google Scholar) with an H-index of 23 (Google Scholar). Among all his papers, there are/were nine ESI Highly Cited Papers. He received the Wang Daheng Optical Prize for Graduate Student from the Chinese Optical Society in 2014, the Young Scientist Awards from the Progress in Electromagnetics Research Symposium in 2018 and 2019, Villum Young Investigator from Villum Fonden in 2021. He is an active reviewer of more than 20 international journals and has received the Publons Peer Review Awards in 2018 and 2019. He was the guest editor of a special issue on metasurface for the journal of *Applied Sciences* in 2018. Now he is the guest editor of a special issue on plasmonic metasurface for the journal of *Photonics*. He has served as an Associate Editor of IEEE *Photonics Journal* since April 2021.